National Oceanography Centre

INTERNAL REPORT

Notes on the Annual and Seasonal Averages of Atmospheric Convection and Changes during the Development of Strong El Niños

David Webb

2025

NOC Internal Report No. 29

Notes on the Annual and Seasonal Averages of Atmospheric Convection and Changes during the Development of Strong El Niños

David J. Webb[1]

[1]National Oceanography Centre, Southampton SO14 3ZH, U.K.

Correspondence: David J. Webb (djw@noc.ac.uk)

Abstract. ERA5 reanalysis data is used to investigate the annual and seasonal average distribution of deep convection in the atmosphere and the changes that occur, especially in the Pacific, during the development of strong El Niños.

The results show that, in normal years, the Inter-Tropical Convergence Zone makes the greatest contribution to the vertical flux at low levels of the atmosphere, but the flux is reduced above 500 hPa. The flux in the Island Continent region is initially lower, but it increases with height so that towards the tropopause the Island Continent becomes the dominant convective region.

During the northern summer, prior to strong El Niños, a much larger fraction of the ITCZ convection penetrates high in the atmosphere. At the same time the vertical flux in the Island Continent region almost halves.

1 Introduction

Recent studies of ocean circulation in the Equatorial Pacific have shown that, during the northern summer, prior to the strong El Niños of 1982-83, 1997-98 and 2015-16, the North Equatorial Counter Current (NECC) conveyed greater amounts of warm water from the west Pacific into the central and eastern Pacific than is normal (Webb, 2018, 2021; Webb et al., 2020). The current lies very close to the latitude of the Inter-Tropical Convergence Zone (ITCZ) and so, at such times, it might be expected to trigger deep atmospheric convection within the ITCZ.

However, although the ITCZ is known to be a region of strong rainfall, and by implication is a region of strong convection, the traditional model of El Niños focuses on the movement of the centre of deep atmospheric convection away from the Island Continent towards the central Pacific (Philander, 1985; Picaut et al., 1996; Clarke, 2014; McPhaden et al., 2020). Given the strong consensus about this, it is unclear what the role of the NECC might be.

To clarify the connections between the different components this paper presents results from a study of vertical fluxes in the Pacific region, with a special emphasis on the areas of deep atmospheric convection. To do this, the study makes use of vertical velocity data from the ECMWF ERA5 reanalysis, for the period 1979 to 2021.

1.1 SST and Convection

In the tropics, the Walker and Hadley Cells and the strength of the atmospheric El Niño depend critically on the strength and location of deep atmospheric convection, defined here as occurring when air rises from near the surface to pressures of 300 hPa or less.

Studies of such events over the ocean (Gadgil et al., 1984; Cubukcu and Krishnamurti, 2002; Evans and Webster, 2014), show that before convection can reach the upper atmosphere, air over the ocean needs to have temperatures above 27°C and be near full saturation.

Kubar and Jiang (2019) made a particular study of the western Pacific and found a similar limit. They also found that the greatest amount of rainfall occurred at sea surface temperatures between 29°C and 30°C.

The critical temperature at each location depends on surface pressure, lower pressures meaning that convecting parcels of air effectively start higher up in the atmosphere. For the same reason deep convection may develop over land at lower temperatures if the topography is high enough. Low pressure may also partly explain why significant cloud and rainfall is also observed along the line of the ITCZ in the central and western Pacific.

Although the study of the Hadley Cell circulation by Dima and Wallace (2003) indicated the importance of the ITCZ regions, the main centre of deep convection in El Niños is usually taken to be the Island Continent. This includes the islands of Indonesia, the Philippines and New Guinea, and may also include parts of south-east Asia and Australia.

Sea surface temperatures in the region are regularly above 27°C. The region also includes rugged islands, so the extra heating associated with island sea breezes and high topography, may be one reason why the Island Continent is such an important deep convection region (Qian, 2008).

However, there remains a discrepancy between deep convection of the Island Continent region, and both the apparent importance of the ITCZ in the Hadley Cell, and the apparent role of the NECC in the development of strong El Niños.

1.2 The ITCZ and the NECC

From the point of view of ocean dynamics, the position of the ITCZ is of interest. The reason it forms north of the Equator in the eastern Pacific is probably due to the blocking effect of the Andes (Takahashi and Battisti, 2007). However, once established the ITCZ becomes a line of low pressure with easterly winds to the north. To the south the winds are generally easterly on the Equator but become more southerly and sometimes westerly as the ITCZ is approached.

The resulting ocean Ekman transport lowers sea level along the line of the ITCZ. In the north, the resulting slope in sea level strengthens the cool westward flowing North Pacific Current. To the south, it generates the North Equatorial Counter Current.

The NECC flows from the west and is anomalous, in the sense that it flows against the general direction of the prevailing winds. It is important because it carries warm west Pacific surface water into the central and eastern Pacific.

In principle the ITCZ and NECC can form a positive feedback loop[1]. In this, warmer than normal sea surface temperatures trigger extra convection, increasing the surface winds and bringing further warm water from the west. It also might reverse the direction of winds along the Equator and so help explain the eastward transport of water on the Equator in the western Pacific that is observed during El Niños.

However, observations indicate that although easterly winds on the Equator adjacent to the ITCZ may be reduced, reversals of the wind field direction are rare. So given the apparent correlation between a warmer than normal NECC and the development of a stronger than normal El Niño, it raises the question, is there some other mechanism by which the higher SSTs can trigger a stronger El Niño, or is the apparent correlation purely fortuitous?

1.3 The Current Study

This paper reports on a study designed to help answer this question by investigating the related processes in the atmosphere. The study is based on the analysis of ERA5 monthly average data sets covering the whole globe. Inevitably there is some overlap with recent papers studying the large scale Walker and Hadley Cells (Guo and Tan, 2018; Feng et al., 2019; Ji et al., 2023; Zhou et al., 2020; Hoskins et al., 2020; Hoskins and Yang, 2021; Held and Hou, 1980; Sun et al., 2019; Li et al., 2023), but the focus here is on the equatorial Pacific and role of the NECC during the development of strong El Niño events.

One of the main results is that, at low levels, the intensity of convection in the ITCZ region is greater than that in the Island Continent/south-east Asia region. The total amount of convection in the ITCZ region is also larger. The differences are greatest in the northern summer months, but the statement is also true for the annual average.

The study also shows that, in the ITCZ region, convection initially increases with height but that the flux drops off at pressures around 500 hPa. In contrast, over the Island Continent the flux is smaller at low levels, but it increases with height, so that at the higher levels of the troposphere it becomes dominant.

During the development of strong El Niños, convection along the line of the ITCZ decreases slightly, but instead of a reduction in flux above 500 hPa, a large fraction of the convective flux continues to near the tropopause. At the same time convection over the Island Continent is severely reduced at all levels.

Section 2 of the paper discusses the ECMWF ERA5 data and the methods used in the reanalysis. Section 3 is concerned with the annual averages during the period 1979 to 2021 and section 4 with averages over the summer and winter months.

Section 5 discusses the effect of the NECC on the ITCZ and the changes that occur during years when a strong El Niño is developing and the core of the NECC is warmer than normal. The final section reviews the results and discusses the possibly causal relationship between the temperature of the NECC and the development of an El Niño.

2 The ERA5 Reanalysis

As models of the climate system improve, reanalysis has been used to provide consistent long-term datasets which can be used to study key climate and weather processes and their impacts. The present study makes use of the monthly average archive data from the ECMWF atmospheric reanalysis, ERA5, (Hersbach et al., 2022) available from the Copernicus data store.

The full dataset covers the period from 1950 to the present, but the results discussed here concentrate on the period from 1979 to 2021. During this period there have been many improvements in the quantity and quality of satellite data, resulting in much better estimates of the state of the atmosphere in remote regions of the globe, such as the equatorial Pacific. The period also includes the strong El Niños of 1982-83, 1997-98 and 2015-16 (Philander, 1983; McPhaden, 1999; Blunden and Arndt, 2016; Santoso et al., 2017).

The atmospheric model used for the ERA5 reanalysis is IFS Cy41r3. An introduction to the model's dynamical core is given by Hortal (2004). Further details of the atmospheric dynamics and physical processes, including the treatment of radiation and convection, are given in the ECMWF on-line documentation (ECMWF, 2016a, b).

2.1 Entrainment

Later in the paper, a number of sections refer to the entrainment and detrainment of air by convective plumes. The convective columns involved are too narrow to be resolved by the ECMWF model and so it uses an improved version of the bulk mass flux scheme described by Tiedtke (1989, 1993)

[1] See Li and Fedorov (2022) but the paper relates sea level change to Ekman velocity instead of Ekman transport.

to represent the process. This represents both updraughts and downdraughts, and allows for a range of convective cell heights within each model cell.

This dependence on a sub-grid scale model is a potential weakness of any study using such data. However, the resulting horizontal divergences of mass and other bulk properties should be constrained by observations. As a result, if the bulk model has significant errors, these should have shown up as a major correction term during the reanalysis.

2.2 Flux formula

The atmospheric El Niño is normally described as occurring when the dominant region of deep atmospheric convection, usually centred over the Island Continent, moves eastwards towards the central Pacific. Such convection involves the movement of air from near the surface to just below the tropopause, i.e. from surface pressures of around 1000 hPa to pressures of 300 to 200 hPa where, near the Equator, the tropopause can reach 17 km.

The ERA5 archive of monthly averaged fields contains data on 17 pressure levels. The present study makes most use of the rate of change of pressure with time experienced by Lagrangian air particles on the 200, 300, 500 and 800 hPa pressure surfaces.

If the atmosphere is in hydrostatic equilibrium, then the vertical pressure gradient dP/dz is given by

$$dP/dz = -g\,\rho, \tag{1}$$

where g is the acceleration due to gravity ρ is the density of air and P is pressure. If the vertical velocity relative to the surfaces of constant pressure (which themself are normally moving) is w_L, then,

$$w_L = \mathrm{d}P_L/\mathrm{d}t \;/\; \mathrm{d}P/\mathrm{d}z, \tag{2}$$

$$= -(1/(g\rho))\,\mathrm{d}P_L/\mathrm{d}t. \tag{3}$$

where P_L is the pressure experienced by a Lagrangian particle. If F_L is vertical mass flux across the moving surfaces of constant pressure, then,

$$F_L = \rho\, w_L, \tag{4}$$

$$= -(1/g)\,\mathrm{d}P_L/\mathrm{d}t. \tag{5}$$

Results are also presented for the overturning mass stream function, calculated from the zonal and time averages of the ERA5 northward component of velocity. The mass stream function Ψ is zero at the top of the atmosphere, so,

$$\Psi(\phi,p) = \int_{z(\psi,\phi,p)}^{\infty} \rho(\psi,\phi,z')\,\overline{v}(\psi,\phi,z')\,\mathrm{d}z'\; R\,cos(\phi)\,\mathrm{d}\psi, \tag{6}$$

$$= (1/g)\int_0^p \overline{v}(\psi,\phi,p')\,\mathrm{d}p'\; R\,cos(\phi)\,\mathrm{d}\psi. \tag{7}$$

where $\overline{v}$ is the time averaged northward component of velocity, ψ is longitude, ϕ latitude, z height, p pressure and R the radius of the Earth.

The reanalysis data shows that, at 500 hPa, the pressure change following a descending particle (dP_L/dt) is of order 0.02 $\mathrm{Pa\,s^{-1}}$. As sea level pressure is around 10^5 Pa, this means that the scale time for descending air in high pressure regions is of order 6×10^6s or 60 days.[2]

The global integral of the flux across each pressure surface is not zero, because the flux does not include precipitation. High in the atmosphere the net flux is small because of the low humidity, but this increases at lower levels. The lower-level pressure surfaces also intersect topography, so especially at short time scales, the total mass of dry air above such surfaces may vary due to pressure changes over the topography.

As a result, at the $500\ \mathrm{hPa}$ level, the vertical flux integral, obtained by integrating globally over all the monthly average data, corresponds to an globally averaged error in dP_L/dt of order $2\times10^{-6}\ \mathrm{Pa\,s^{-1}}$. This is much smaller than the values of Fig. 1. However, lower in the atmosphere, at $800\ \mathrm{hPa}$, the mismatch increases to order $3\times10^{-3}\ \mathrm{Pa\,s^{-1}}$.

Over land the ERA5 pressure tendency fields contain small-scale sign-changing noise, often associated with trends in the underlying topography. The reason for the noise is not known but it may reflect the regular presence of standing atmospheric waves. For the results presented here, the values on the model grid were averaged by twice applying a 3 grid point by 3 grid point box filter. This slightly reduces the noise apparent in the figures. It also reduces the area averages of rising and descending air, discussed later, by a few per cent.

3 Long-term Average

Figure 1, shows the long-term average of the vertical flux across the 300, 500 and 800 hPa pressure surfaces calculated from the ERA5 monthly average data between 1979 and 2021. Over the oceans, convection is strongest along the line of the Pacific ITCZ, with lesser values in the equatorial Atlantic, in the South Pacific Convergence Zone (SPCZ) and south of the Equator in the Indian Ocean.

At $800\ \mathrm{hPa}$, convection over the seas of the Island Continent is surprisingly weak. Bands of weaker convection are also associated with the storm tracks in the North Pacific, North Atlantic and Southern Oceans.

The regions of sinking air over the oceans correspond to the sub-tropical oceanic gyres of the North and South Atlantic, North and South Pacific and the southern Indian Ocean. Maximum sinking rates occur on the eastern boundary of each of these regions, around 30° north or south, the latitudes corresponding to the normally accepted limits of the overturning Hadley cells.

In the Pacific, a third sinking region can be identified, lying on the Equator and separated from the South Pacific region by a band of lower vertical velocities. The Coriolis term in this region is small, so assuming the ERA5 results are realistic, this is the downward branch of the Walker Cell, also known as the Pacific Equatorial Dry Zone (Hastenrath, 1999).

[2] In terms of mass fluxes, 0.02 $\mathrm{Pa\,s^{-1}}$ corresponds to a mass flux F_L of ~0.002 $\mathrm{kg\,m^{-2}\,s^{-1}}$. Integrated globally this becomes ~10^{12} $\mathrm{kg\,s^{-1}}$. The total mass of the atmosphere is ~5.15 10^{18} kg so again the time scale is of order 60 days.

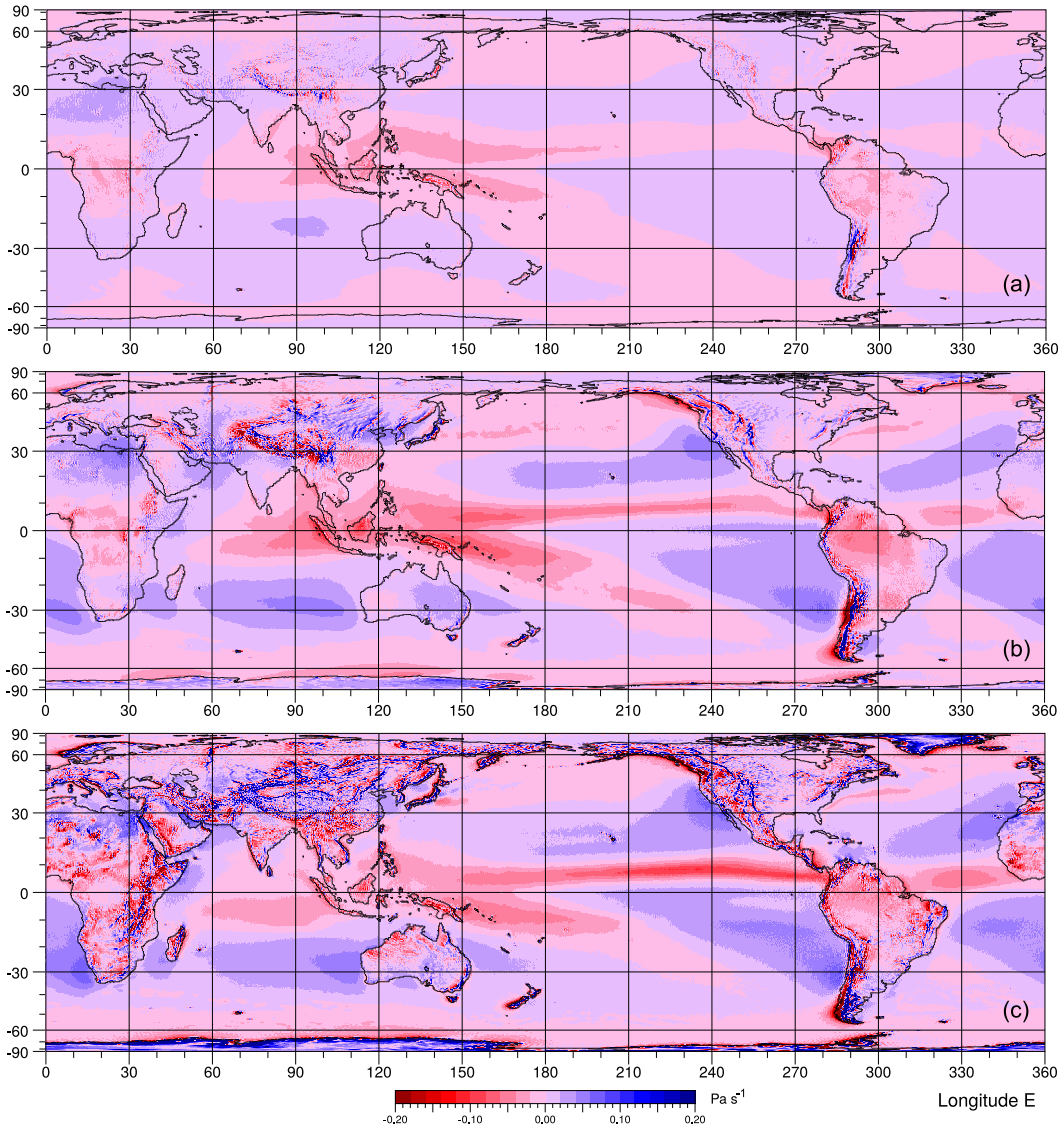

Figure 1. The average rate of change of pressure following particles crossing the (a) 300 hPa, (b) 500 hPa and (c) 800 hPa pressure surface during the years 1979 to 2021 inclusive (units $\mathrm{Pa\,s^{-1}}$). Negative (red) values correspond to rising air. The projection is Lambert equal-area.

In contrast to the oceans, over which the vertical velocities vary smoothly with position, vertical velocities over the continents are dominated by the short wavelength features discussed earlier. Amplitudes appear to be greatest around regions of steep topography.

This short wavelength 'noise' may be result of numerical errors in the model, but it is most noticeable in regions of ascending air, so it could also be the result of the numerical model's representation of convection triggered by topography.

Over land, the main convections regions include South America, Central Africa, India and south-east Asia. Sinking regions include North Africa, parts of Arabia and Siberia, much of Canada and parts of Greenland and Antarctica.

3.1 Changes with Height

At 500 hPa, the middle of the three levels shown, convection in the central and eastern Pacific sector of the ITCZ is reduced. It is also reduced in the Atlantic sector.

Instead, the main areas of convection are now the western Pacific, north and south of the Equator, and the Island Continent region, where the latter has an extension into the eastern Indian Ocean.

There are also changes in the regions of sinking air over the ocean, with a possible tendency for the largest values to move towards the centre of each ocean.

Over land the intensity of convective noise is reduced but, qualitatively, the flux of sinking air appears less affected.

At 300 hPa, near the tropopause, the vertical fluxes are all reduced. The main centre of convection is now the Island Continent. This has extensions into the Pacific, north and south of the Equator, and into the Indian Ocean. Less

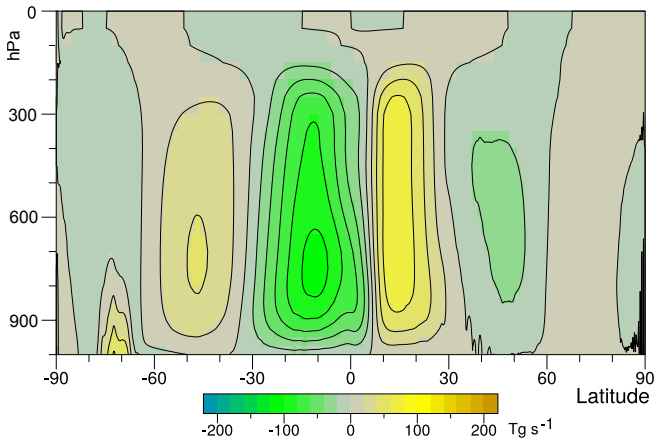

Figure 2. The overturning stream function calculated from the zonally averaged velocities averaged between 1979 and 2021. The contour separation is 20 $\mathrm{Tg\,s^{-1}}$ (20 $\times 10^9$ $\mathrm{kg\,s^{-1}}$).

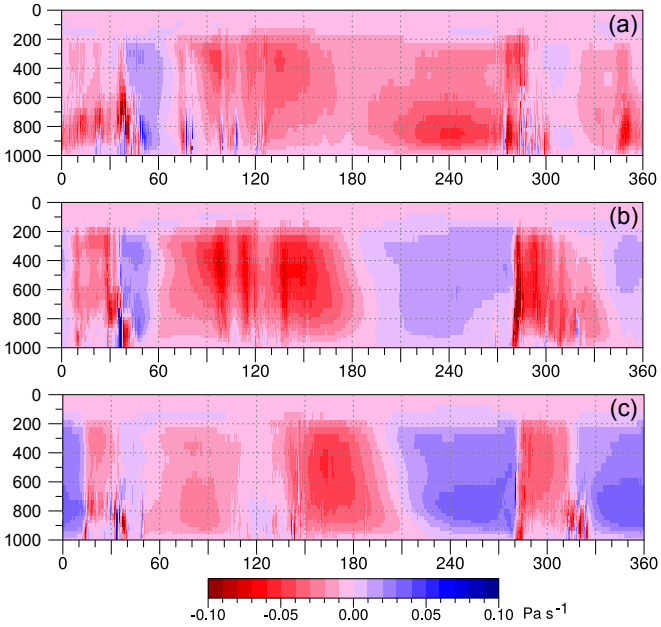

Figure 3. Average value of the Lagrangian particle velocity, across pressure surfaces, in the bands between (a) 5°N and 15°N, (b) 5°S and 5°N and (c) 15°S and 5°S, during the period 1979 to 2021. Note the change in colour scale from the equal-area plots.

important regions of convection are found over Equatorial Africa and the Amazon rainforest.

The pattern of sinking air is similar to the patterns seen lower in the atmosphere, but there are noticeable maxima in the Indian Ocean, near 20°S, and over north Africa.

3.2 The Zonal Average

In the past, discussion of the general circulation of the atmosphere has often focussed on the zonally averaged overturning stream function. The stream function calculated from the ERA5 data between 1979 and 2021, is plotted in Fig. 2. It shows the classic Hadley cells extending from near the Equator to 30°north and south. The Ferrell Cells then extend to 60° and are followed by weak features closer to the poles.

The boundary between the two Hadley Cells lies not on the Equator but near 7°N, close to the line of the ITCZ. The offset was first reported by Lindzen and Hou (1988) based on air soundings summarised by Oort and Rasmusson (1970). Later Dima and Wallace (2003) reported an similar offset in the NCAR-NCEP reanalysis data[3].

In the case of the northern cell, the rising branch covers only the small range of latitudes between 7°N and 15°N. In the vertical, the flux increases between 1000 hPa and 800 hPa, but then remains almost constant, around 60 $\mathrm{Tg\,s^{-1}}$, up to the 250 hPa level. This may be unexpected given the reduced convection over the ITCZ seen earlier.

The Hadley Cell south of the Equator has a much broader rising branch, extending to 10°S. Near the ground there appears to be some structure, below 850 hPa close to the Equator, but above this there is evidence of two separate cells.

In the first of these, a flux of 40 $\mathrm{Tg\,s^{-1}}$ is carried past the 750 hPa level before flowing south in a broad band extending from 750 hPa to beyond 400 hPa. Above this, a second cell, similar in strength to the northern Hadley Cell, carries a flux of 60 $\mathrm{Tg\,s^{-1}}$ up to pressures around 250 hPa. Then, as with the northern cell, the flow away from the convection region is concentrated in a relatively narrow band of pressure.

3.3 Sections near the Equator

Fig. 3 provides further detail on how vertical velocities change with pressure, in three bands near the Equator. The first, in which the vertical velocities are averaged between 5°N and 15°N, corresponds roughly to the ITCZ. The second, which averages from 5°S to 5°N, covers the equatorial band where the Coriolis force is small. The third, from 15°S to 5°S, includes part of the SPCZ.

The northern band shows that over the central and eastern Pacific, the convection associated with the ITCZ is strongest between the surface and 600 hPa. Above this, the convective flux remains positive up to the tropopause, implying that the ITCZ includes a limited amount of deep convection. Similar behaviour is seen over part of the Atlantic and over Africa.

This pattern is in strong contrast to that over the Island Continent and nearby seas. Here convection at low levels is very weak, but it increases with height to a maximum high in the atmosphere. Over Central America there is a maximum in convective activity below 700 hPa and a second maximum near 300 hPa.

In the Equatorial band, the descending branch of the Walker Cell, shows up clearly in the central and eastern Pacific where air descends from the tropopause to the ocean surface.

Convection over the Island Continent is also different. At the 900 hPa level convection is less than in the ITCZ region of the eastern Pacific. The flux then increases with height up to 700 hPa, after which it remains relatively constant as far as the tropopause.

[3]NCEP-NCAR: National Centers for Environmental Prediction-National Centre for Atmospheric Research.

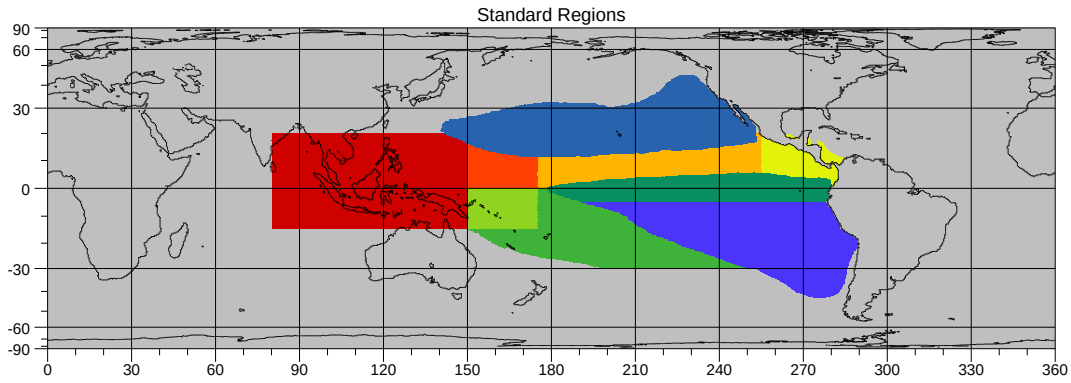

Figure 4. Standard zones used in Table 1. The zones are Island Continent, dark red; ITCZ (West), red; ITCZ, orange; EPCZ, yellow; SPCZ (West) light green; SPCZ, green; Equator, dark green; N. Pacific, grey blue; S. Pacific, blue.

This region of strong convection also extends towards the central Pacific and the central Indian Ocean. Throughout the region vertical velocities at mid-levels are generally much higher than those in the 5°N to 15°N band.

A similar pattern is observed over Africa. When compared to the bands to the north and south, convection at low levels is weak, but it increases above 700 hPa level with an indication of a double maxima in the vertical flux.

South America, near the Andes, also shows strong vertical transport from 800 hPa to 250 hPa, the lower level probably being related to the height of topography.

In the final section, south of the Equator, the main area of rising air corresponds to the South Pacific Convection Zone (SPCZ). Here the convective flux increases with height, but maximum values are generally less than near the Equator. Over the Indian Ocean, convection has a maximum around 700 hPa, but here, and over Africa and South America, some of the convection reaches the 250 hPa level.

In this southern band, the main sinking regions are found in the eastern Pacific and the Atlantic with a significant increase in the rate at which air sinks between 600 hPa and 850 hPa

Table 1. Mass fluxes across standard pressure levels, averaged over the period 1979 to 2021 inclusive and integrated over the standard zones of Fig. 4. Positive values indicate a net downward motion. The mass flux units are $\mathrm{Tg\,s^{-1}}$

Pressure	200 hPa	500 hPa	800 hPa
Island Continent	−52.39	−86.93	−51.65
ITCZ (West)	−7.68	−14.99	−11.40
ITCZ	−8.75	−23.97	−40.10
EPWP	−3.78	−8.21	−15.86
SPCZ (West)	−9.38	−20.68	−16.70
SPCZ	−10.11	−26.98	−14.29
Equator	10.62	17.69	13.95
North Pacific	12.56	43.90	52.41
South Pacific	22.58	57.83	58.14
World	−0.02	−0.13	156.54

3.4 Quantitative Fluxes

These results show, qualitatively, that the overturning circulation is not as simple as often envisaged but that it consists of low-level convection in some areas of the globe and high-level convection elsewhere.

The focus of this paper is on the Pacific, so here in order to be quantitatively precise, the ascending and descending fluxes are calculated for each of the regions illustrated in Fig. 4.

The regions, based on the 500 hPa level of Fig. 1, consist of the Island Continent, the ITCZ and SPCZ, the cold-water equatorial band, the descending regions of the North and South Pacific and three extra regions. The first of these is the East Pacific Convection Zone (EPCZ) which lies above the eastern Pacific warm pool. The other two are treated separately because they lie adjacent to the Island Continent and might be considered to be extensions of the Island Continent or part of one of the convergence zones.

Table 1 gives the average mass flux of air crossing the 200, 500 and 800 hPa levels integrated over the standard zones and over the whole analysis period. Values were calculated, using Eqn. 4, to convert the ERA5 data into mass fluxes.

The table shows that Island Continent region provides the greatest contribution to convection at all three levels. However, it is not as dominant as might be expected. At the lowest level, 800 hPa, when compared with the Island Continent value, the three ITCZ zones contribute an additional 130% and the two SPCZ zones contribution additional 60% to the total. This agrees with the earlier figures, which indicate that at low levels the Island Continent is important but not dominant.

At 500 hPa, the flux in the Island Continent region has increased by two-thirds. This could be due, in part, to topography over 5,000 m, but is most likely due to entrainment by convection. Fluxes also increase in the western parts of the ITCZ and SPCZ, and almost double in the main SPCZ region. The area of high mountains in these regions is limited, so entrainment is the probable cause.

However, the convective fluxes in the East Pacific Warm Pool (EPWP) and the two ITCZ zones almost halve, indi-

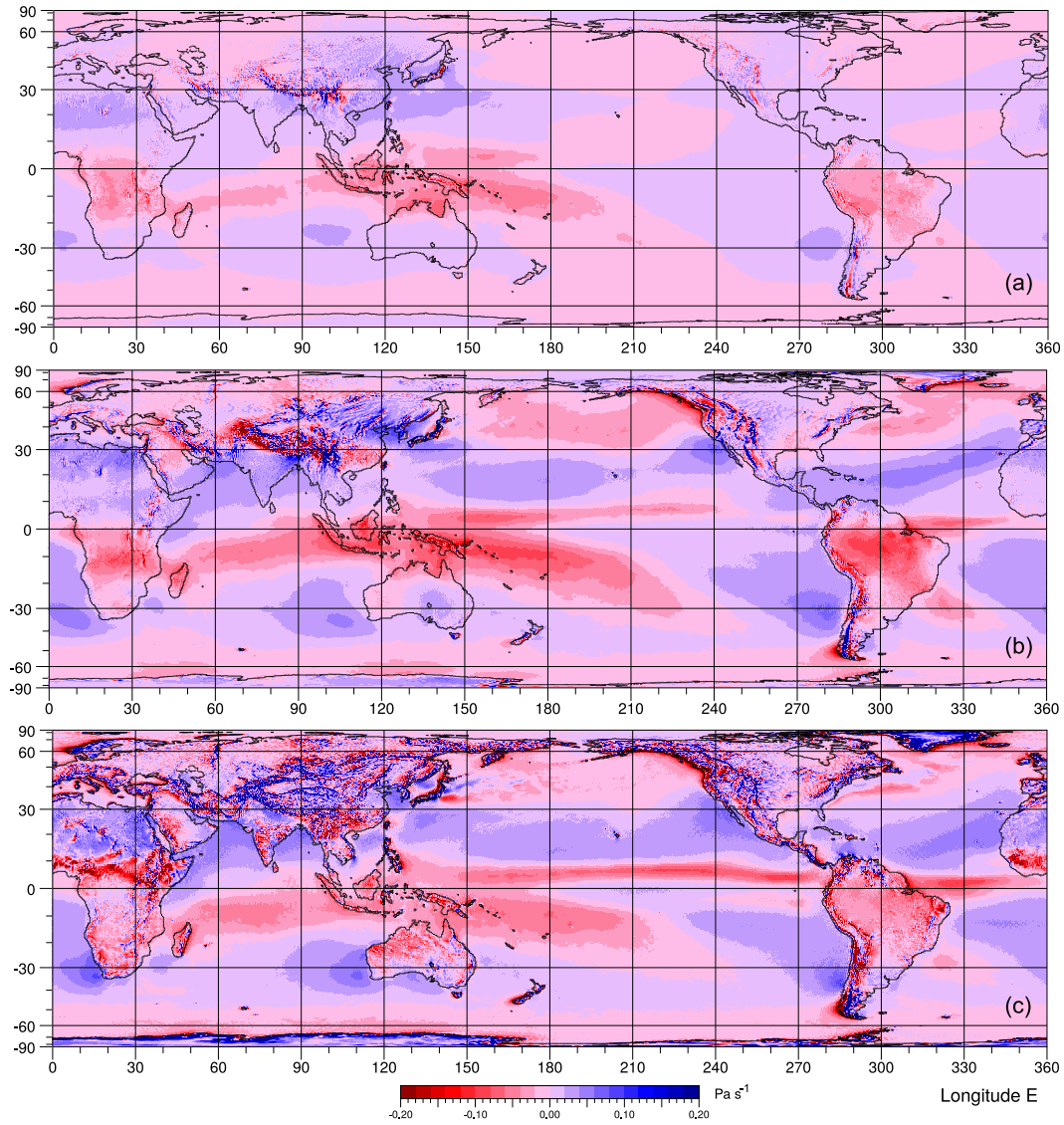

Figure 5. The average rate of change of pressure following particles crossing the (a) 300, (b) 500 and (c) 800 hPa pressure surfaces during January, February and March, during the period 1979 and 2021 inclusive.

cating that in the middle atmosphere the central and eastern Pacific ITCZ zones become a region of divergence.

Near the top of the troposphere, at 200 hPa, the Island Continent remains the dominant convective region. However, all of the other convective regions still show a net upward flux of air, their total contribution being 75% of the Island Continent value.

In regions where, on average, the air is descending, the South Pacific dominates at all levels. At 800 and 500 hPa, the North Pacific contribution is slightly less but at 200 hPa it drops to just over half of the South Pacific value. Near the surface, the Cold Pool contribution is relatively small, but the flux of sinking air increases higher in the atmosphere. At 200 hPa sinking over the Cold Pool is only slightly less than in the much larger North Pacific zone.

4 Seasonal Changes

Seasonal changes in solar heating, result in significant changes in the pattern of convection. This is illustrated by Figs. 5 and 6 which show the vertical flux of air at the three levels used previously, averaged over the months January to March and July to September. The zonally averaged stream functions for the same periods are shown in Fig. 7 and the vertical fluxes, in the three zonal bands, in Figs. 9 and 10. Net fluxes, in the standard zones during the same periods, are given in Tables 2 and 3.

The ERA5 analysis indicates that, during the northern winter, convection over the Island Continent is concentrated south of the Equator and that it moves north of the Equator during the northern summer. Table 2 shows that in winter, the vertical flux is 46 $\mathrm{Tg\,s^{-1}}$ at 800 hPa, increasing to around 75 $\mathrm{Tg\,s^{-1}}$ in the middle atmosphere, but dropping back to 46 $\mathrm{Tg\,s^{-1}}$ again at 200 hPa.

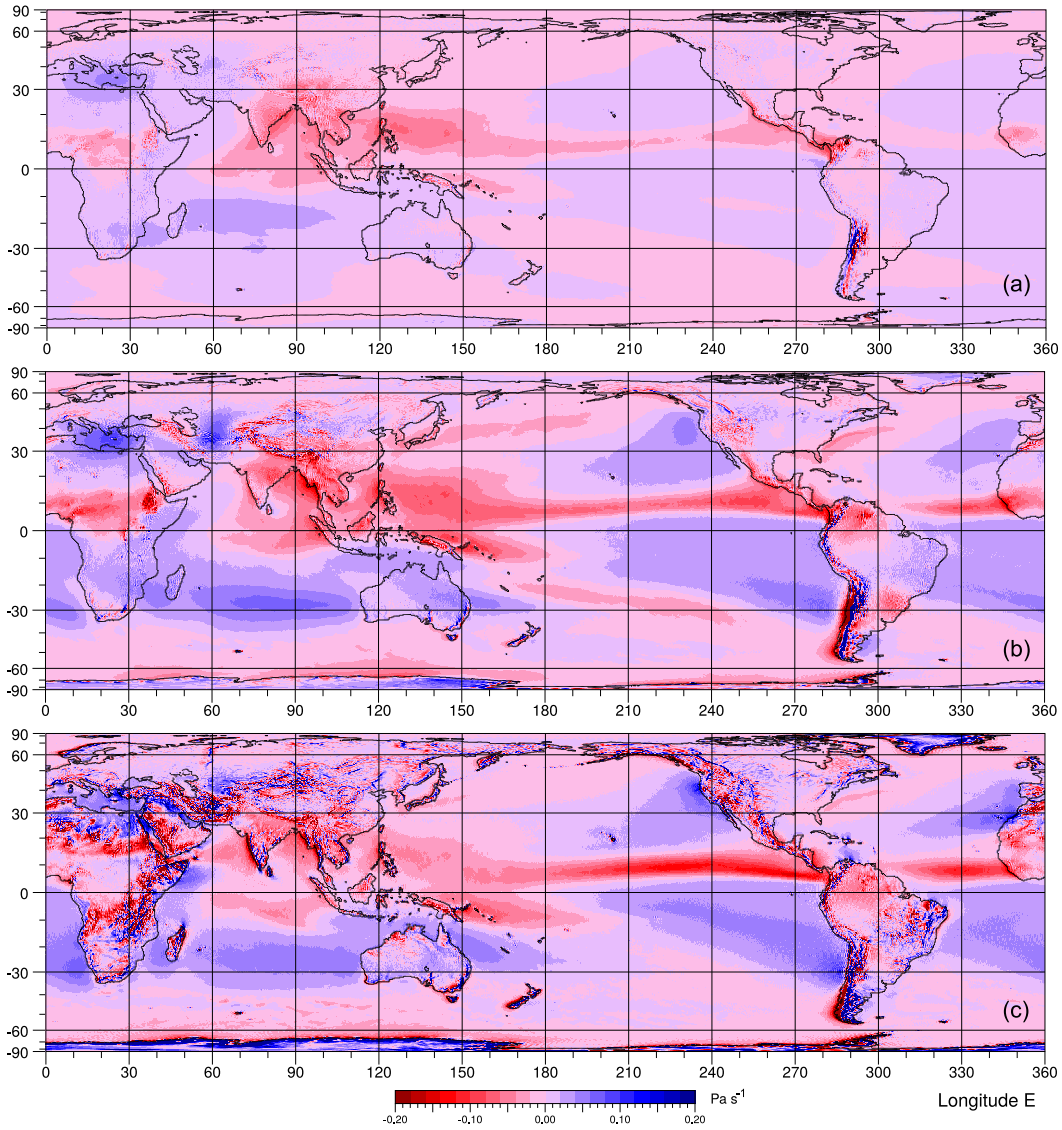

Figure 6. The average rate of change of pressure following particles crossing the (a) 300, (b) 500 and (c) 800 hPa pressure surfaces during July, August and September, during the period 1979 and 2021 inclusive.

Vertical fluxes increase significantly during the northern summer (Table 3), the greatest percentage increase occurring in the middle atmosphere where the flux reaches ~104 $\mathrm{Tg\,s^{-1}}$. In summer the vertical flux at 200 hPa is also significantly larger than at 800 hPa.

Over the Pacific Ocean, there are large seasonal changes in the strength of convection connected to the ITCZ and SPCZ. Convection along the ITCZ is strongest during the northern summer, the total flux at 800 hPa having a value of 73 $\mathrm{Tg\,s^{-1}}$, significantly greater than the total in the Island Continent zone.

However, the flux drops to 56 $\mathrm{Tg\,s^{-1}}$ in the middle atmosphere and to 21 $\mathrm{Tg\,s^{-1}}$ at 200 hPa. Fluxes are also significantly reduced during the northern winter, but again the fluxes are greatest at 800 hPa and become significantly reduced higher in the atmosphere.

During the northern summer, convection over the East Pacific Warm Pool is also significant. At 800 hPa the flux is 26 $\mathrm{Tg\,s^{-1}}$, exceeding 50% of the Island Continent value at 800 hPa. The values drops slightly to 22 $\mathrm{Tg\,s^{-1}}$, in the middle atmosphere, and then to 10 $\mathrm{Tg\,s^{-1}}$ at 200 hPa.

South of the Equator, the strongest convection over the SPCZ occurs, as expected, during the southern summer. As in the Island Continent region, this has a maximum in the middle atmosphere, the total reaching 85 $\mathrm{Tg\,s^{-1}}$, exceeding the Island Continent value. At 800 hPa the SPCZ flux, 57 $\mathrm{Tg\,s^{-1}}$ also exceeds the Island Continent value, but higher in the atmosphere the flux diminishes, dropping to 41 $\mathrm{Tg\,s^{-1}}$, slightly less than the Island Continent value.

4.0.1 Net Sinking Regions

Figures 5 and 6 also show significant seasonal changes in the net sinking regions.

In the North Pacific, at 800 and 500 hPa the total area involved, and the sinking rates are much greater during the

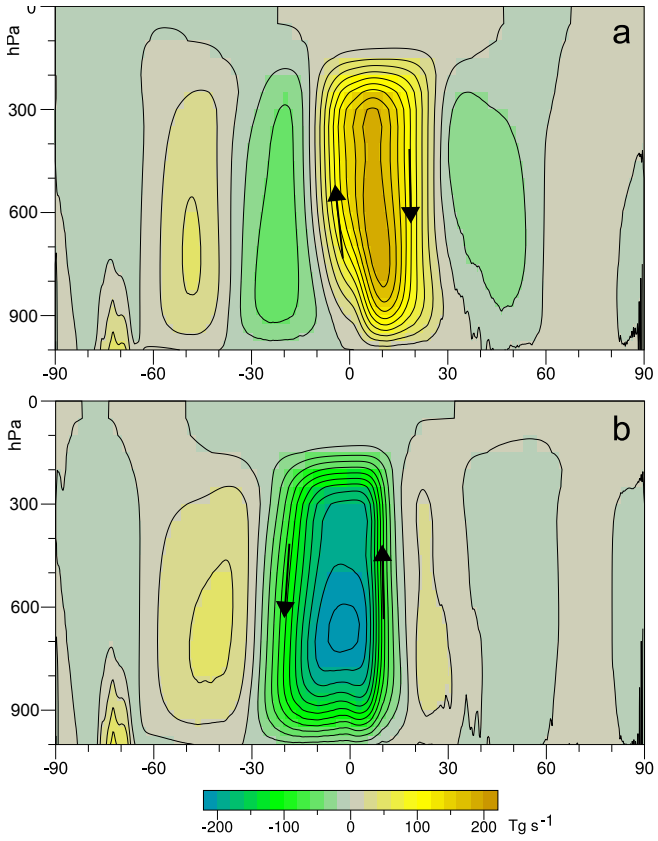

Figure 7. The overturning zonal stream function averaged over (a) January to March and (b) July to September, during each year between 1979 and 2021. The contour separation is 20 $\mathrm{Tg\,s^{-1}}$ (20 $\times 10^9$ $\mathrm{kg\,s^{-1}}$).

northern winter than during the summer months. However, at 300 hPa the position is reversed with both the area involved and the sinking rate appearing greater in summer than winter.

In the South Pacific, the sinking rates and areas involved are largest during the southern winter at all levels. At this time the South Pacific region is also linked to the Equatorial Cold Pool, but the link is broken during the southern summer by a line of net convection just south of the Equator.

The quantitative fluxes summarised in Tables 2 and 3, confirm this behaviour but show some interesting detail. Both the North and South Pacific regions show the largest downward fluxes during the corresponding winter period, with the fluxes being a maximum at the lowest level, 68 $\mathrm{Tg\,s^{-1}}$ in the North Pacific, 76 $\mathrm{Tg\,s^{-1}}$ in the South Pacific and 29 $\mathrm{Tg\,s^{-1}}$ in the Cold Pool.

However, during the southern summer, both the South Pacific and the Cold Pool region have maximum sinking rates in the middle atmosphere. This may be associated with the barrier region mentioned previously, a real or model induced mirror of the ITCZ to the north.

4.1 The Overturning Stream Functions

The overturning stream functions for the northern winter and summer periods are shown in Fig. 7. In both cases, the figures indicate that entrainment into the main Hadley Cell, is active up to a level around 800 hPa. The main sinking branch is also in the winter hemisphere, extending to 30° north or south.

However, convection near the ground does not follow the seasons. In both cases the stream function lines show that near the ground, the vertical motion, averaged along lines of latitude, is concentrated north of the Equator.

During the July to September period, the stream-lines in the convective region are almost vertical. In contrast, during the January to March period, although convection starts north of the Equator, a significant portion of the total flux moves south of the Equator at pressures between 900 and 600 hPa.

If all deep atmospheric convection occurred in single massive clouds or cloud groups, then the stream-lines in both seasons would be vertical. What is unusual here is that, during the southern summer, the convective stream-lines move across the Equator. As individual clouds and cloud groups do not have this behaviour, it means that entrainment by clouds south of the Equator, must match the detrainment by clouds to the north.

During this period, the maximum value of stream function lies between 180 and 200 $\mathrm{Tg\,s^{-1}}$. This is comparable to the values estimated by Oort and Yienger (1996) based on rawinsonde data. In both sets of results the rising branch of the Hadley Cell lies in a narrow region close to 10°N. They also show that almost all the Hadley Cell convective inflow occurs at pressures above 800 hPa and most of the outflow occurs at pressures less than 300 hPa.

In the July to September period, the stream function maximum increases to over 220 $\mathrm{Tg\,s^{-1}}$, but much of the increase comes from air that does not reach the 300 hPa level. This implies that, during these months, the more penetrative clouds are not entraining all the air detrained by clouds at lower levels.

The effect of entrainment in the middle atmosphere is illustrated in Fig. 8, which shows the average difference in the fluxes at 700 and 300 hPa during the late summer and the integrated flux along the band between 5°N and 12°N during the same period. The band is chosen because it includes the regions of excess low-level convection in both the Pacific and Atlantic Oceans.

The results show that the net vertical flux a both 700 and 300 hPa is around 140 $\mathrm{Tg\,s^{-1}}$. Thus, this relatively narrow band contributes to around 70% of the total Hadley circulation between July and September.

Figure 8b shows that in the Indonesian region, the total flux at 300 hPa is made up of half coming from the flux at 700 hPa and half by entrainment in the middle atmosphere. In the central Pacific there is an excess in convection at low levels leading inevitability to detrainment in the middle atmosphere. As a result, by the time the eastern Pacific is reached, the two effects are in balance, the total detrainment over the Pacific just balancing the entrainment over Indonesia.

Further east a similar balance is apparent, the excess detrainment at mid-levels over the Atlantic just balancing the extra entrainment over the Americas and Africa. Overall, as was seen in Fig. 7, not everything balances out but, given the diversity of the regions involved, they have an unexpectedly close relationship.

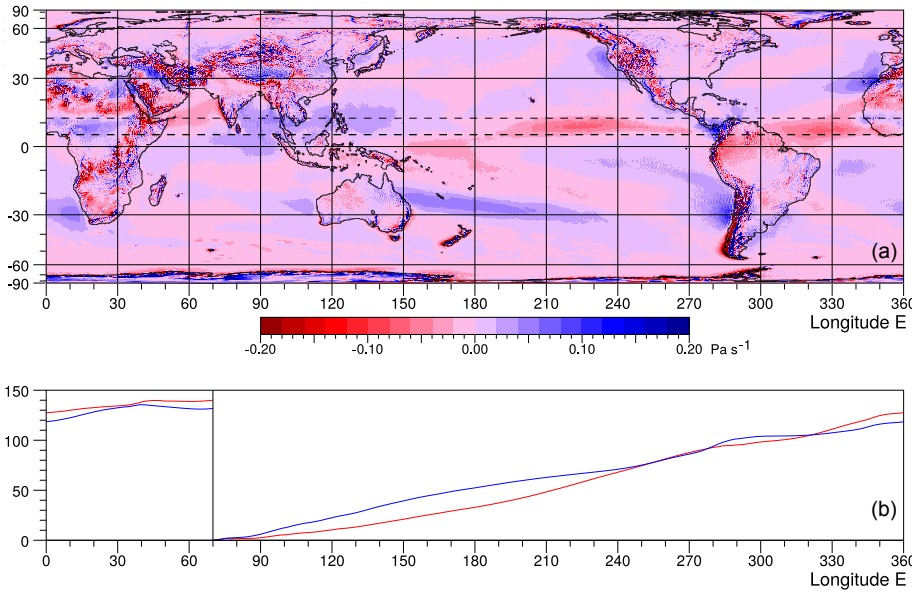

Figure 8. (a) The difference in the vertical flux between 300 hPa and 700 hPa averaged over months July, August and September in each year from 1979 to 2021. (b) Longitudinal integral of the vertical mass flux ($\mathrm{Tg\,s^{-1}}$) for the 700 hPa (red) and 300 hPa (blue) levels, calculated for the same time averaging period and integrated between 5°N and 12°N, and eastwards from 70°E to the longitude plotted.

Table 2. Mass fluxes across standard pressure levels, averaged over the months January, February and March of years 1979 to 2021, and integrated over the standard zones of Fig. 4. The mass flux units are $\mathrm{Tg\,s^{-1}}$

Pressure	200 hPa	500 hPa	800 hPa
Island Continent	−46.09	−75.66	−46.03
ITCZ (West)	−6.18	−9.09	−8.64
ITCZ	−2.78	−11.48	−19.73
EPWP	3.51	7.34	−1.70
SPCZ (West)	−17.59	−30.38	−20.32
SPCZ	−22.96	−53.53	−37.07
Equator	8.43	9.43	−6.16
North Pacific	9.36	48.66	68.07
South Pacific	28.30	51.58	44.58
World	−0.04	−0.19	160.01

Table 3. Mass fluxes across standard pressure levels, averaged over the months July, August and September of years 1979 to 2021, and integrated over the standard zones of Fig. 4. The mass flux units are $\mathrm{Tg\,s^{-1}}$

Pressure	200 hPa	500 hPa	800 hPa
Island Continent	−62.60	−104.14	−51.24
ITCZ (West)	−8.67	−20.81	−13.83
ITCZ	−12.14	−35.08	−59.66
EPWP	−9.55	−22.58	−26.44
SPCZ (West)	−3.98	−15.44	−16.96
SPCZ	−1.43	−8.67	4.30
Equator	14.07	27.26	29.20
North Pacific	10.71	27.57	32.48
South Pacific	15.89	68.82	76.43
World	−0.02	−0.09	152.44

4.2 Convection in the Zonal Bands

The seasonal variations in the zonal bands discussed earlier are shown in Figs. 9 and 10.

In the January to March period, convection over the Pacific in the 5°N to 15°N section, is weak, although some rising air does reach the tropopause. Around the Equator, there is some convection in the eastern Pacific at low levels, but most convection occurs over the Island Continent, the eastern Indian Ocean, Africa and South America. In each of these areas, the convection is also penetrating high into the atmosphere.

In the band between 15°S and 5°S, the dominant convection region includes both the Island Continent and the SPCZ, in agreement with the values of Table 3. The figure also shows the vertical flux here and over South America increasing with height. Following the overturning stream function result this is likely to be the result of entrainment from further north.

During this period, and within the three zones, the main areas with sinking air are the eastern South Pacific and the South Atlantic. In both cases there are regions with a maximum in the sinking rate around 800 hPa, but elsewhere the behaviour is more complex, the eastern Equatorial Pacific showing air sinking above 500 hPa and convection below.

A different picture emerges during the July to September period. North of the Equator, the eastern Pacific shows the region of low-level convection seen in the annual average, but here the flux is larger and more of the flux continues to the tropopause where there is a secondary flux maximum. Similar maxima are also seen near 300 hPa over the Island Continent and the eastern Indian Ocean.

In the equatorial band, a major feature is the sinking region over the Equatorial Cold Pool and its continuation into the South Pacific. The Island Continent region remains a re-

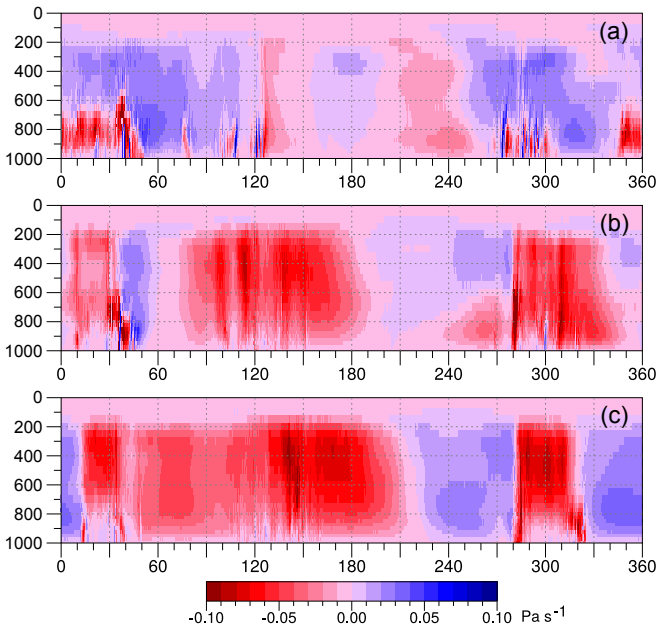

Figure 9. Average value of the Lagrangian particle velocity between (a) 5°N and 15°N, (b) 5°S and 5°N and (c) 15°S and 5°S, during the months January, February and March of years 1979 to 2021 (units $\mathrm{Pa\,s^{-1}}$). Negative (red) values correspond to rising air.

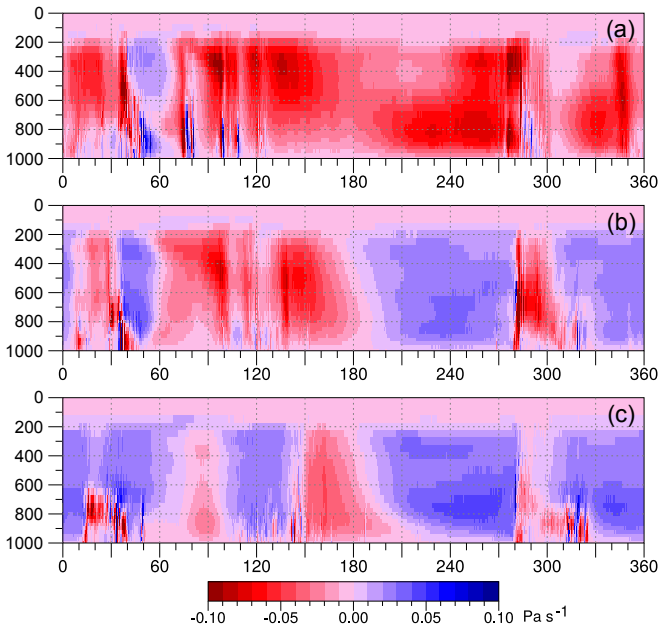

Figure 10. Average value of the Lagrangian particle velocity between (a) 5°N and 15°N, (b) 5°S and 5°N and (c) 15°S and 5°S, during the months July, August and September of years 1979 to 2021 (units $\mathrm{Pa\,s^{-1}}$). Negative (red) values correspond to rising air.

gion of net convection, as does the eastern Indian Ocean, but further south, the seas north of Australia become a region of net sinking.

Overall, the results indicate that at low levels, the Island Continent is just one of many regions where significant convection occurs, with the SPCZ being more significant during the January to March and the ITCZ during July to September.

However, moving higher in the atmosphere, the Island Continent region starts to dominate convection, the results of this and the previous section indicating that this is due to entrainment of air at mid-atmospheric levels.

5 Convection, the ITCZ and the NECC

As discussed earlier, studies of strong El Niños showed that during the El Niño growth phase, the NECC carried unusually large amounts of warm water into the central and eastern Pacific.

The path of the NECC usually lies just south of the Pacific ITCZ. As shown in the previous section, the ITCZ makes a significant contribution to convection in the lower atmosphere, especially during the norther summer. What changed during the development of the strong El Niños was that ocean temperatures, in the central Pacific section of the current, rose above 28°C. As discussed earlier such temperatures are critical for the development of deep atmospheric convection. It is thus possible that the normal convective activity along the path of the ITCZ changed and that convective plumes rose much higher in the atmosphere.

To see if this is the case, the previous analysis was repeated but for just the summer months of 1983, 1997 and 2015. This is the period during the growth of the El Niños when the

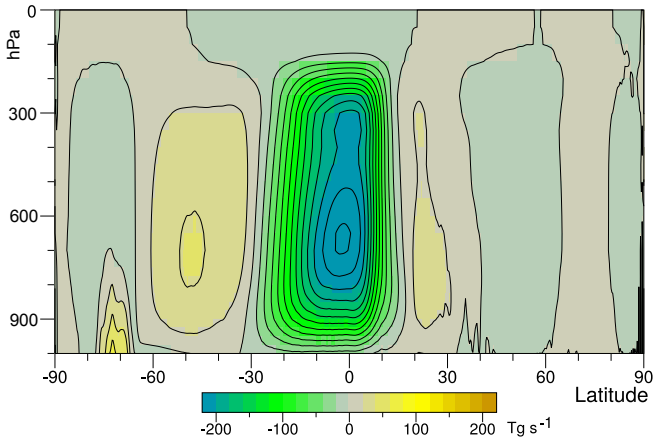

Figure 11. The overturning zonal stream function averaged over July, August and September of years 1982, 1997 and 2015. The contour separation is 20 $\mathrm{Tg\,s^{-1}}$ (20×10^9 $\mathrm{kg\,s^{-1}}$).

warm NECC water was crossing the central Pacific, and the corresponding patches of warm water on the Equator were still far to the west.

5.1 The Hadley Cell

Figure 11 shows the zonally averaged overturning stream function during the development of the strong El Niños. Comparison with Fig. 7 shows that the main change is a small increase in the overturning flux crossing the 300 hPa level.

However, the difference in the fluxes at 700 and 300 hPa (see Fig. 14), shows much greater differences. During the strong El Niños, the divergence in the eastern Pacific low-level flux is reduced and, as a result, the excess detrainment

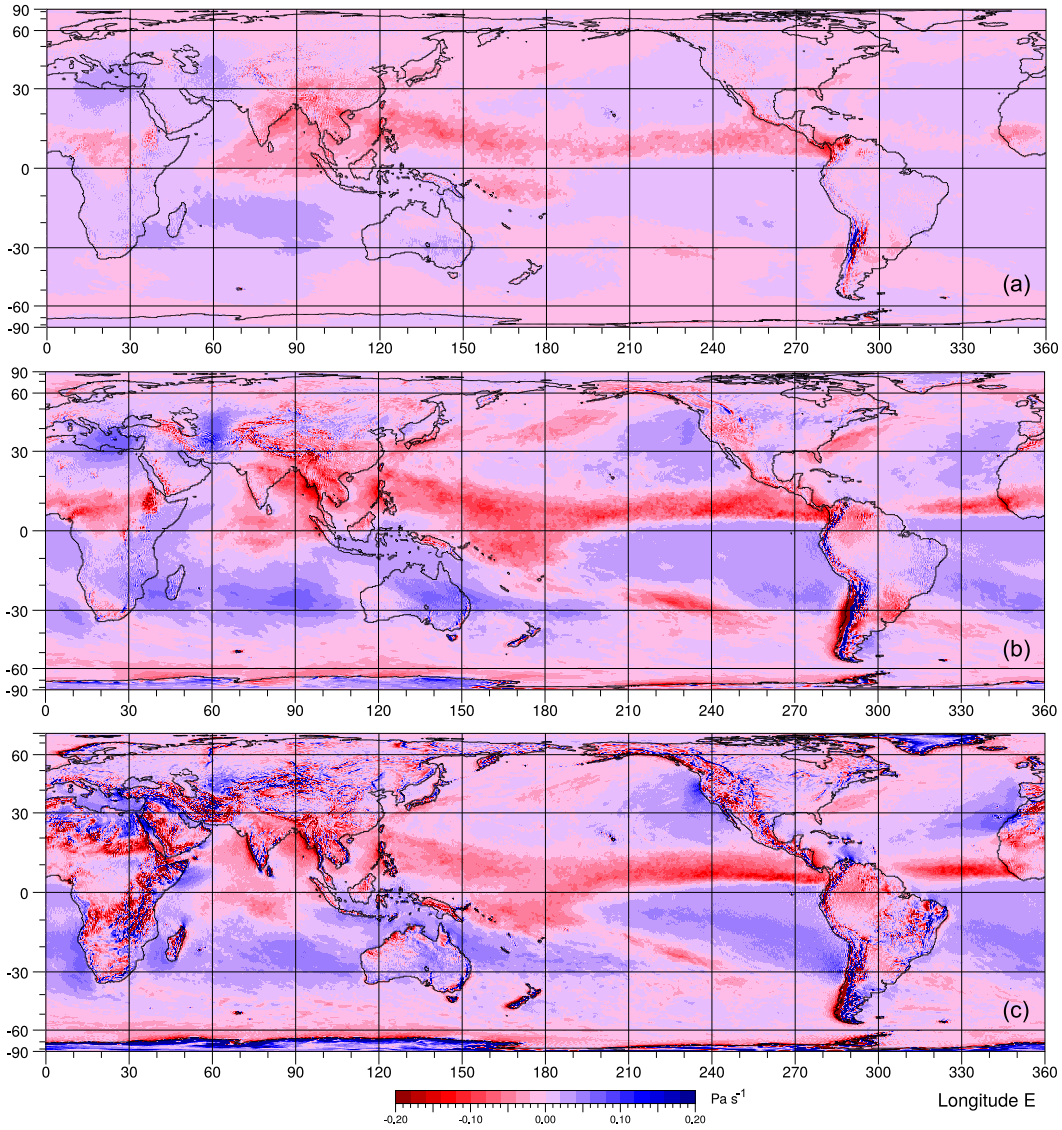

Figure 12. The average rate of change of pressure following particles crossing the (a) 300, (b) 500 and (c) 800 hPa pressure surfaces during July, August and September of years 1982, 1997 and 2015.

at the mid-levels is no longer sufficient to balance entrainment in the Island Continent region.

Instead a comparison with Fig. 14a, shows that during the strong El Niños there is an increase in low level convection within the Atlantic sector. Figure 14b showing that this is sufficient to compensates for the reduced low-level convection in the central and eastern Pacific.

Thus what appeared to be a small change in the strength of the Hadley Cell, is a result of a possibly unexpected balance between convection in the Island Continent, ITCZ and the equatorial Atlantic regions.

5.2 Flux crossing Pressure Surfaces

A comparison of the fluxes crossing the 800 hPa pressure surfaces (Figs. 6 and 12) shows that during the development of strong El Niños there are other potentially important changes.

Possibly the most significant of these is concerned with the region of convection close to New Guinea and the region of sinking air over northern Australia. During the development of the strong El Niños, much of the convection associated with New Guinea moves eastwards, with the northern Australian region of sinking air expanding both northwards and eastwards.

These movements also appear to affect the equatorial atmosphere north of New Guinea. Usually there is a convective patch centered near 150°E, but during the northern summer when strong El Niños are developing, this moves eastwards. It is this movement which is conventionally used to describe how the atmospheric component of El Niños develop.

Further north, vertical fluxes at latitudes between 10°N and 20 °N are also affected, with convection extending further eastwards than normal. In the central and eastern Pacific, the ITCZ becomes stronger along its southern boundary, which itself moves towards the Equator

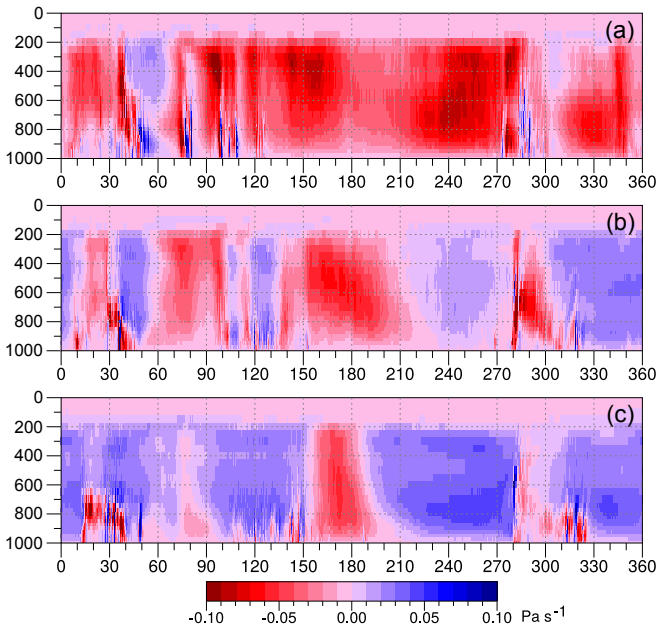

Figure 13. Average value of the Lagrangian particle velocity between (a) 5°N and 15°N, (b) 5°S and 5°N and (c) 15°S and 5°S, during July August and September of years 1982, 1997 and 2015 (units $\mathrm{Pa\,s^{-1}}$). Negative (red) values correspond to rising air.

Table 4. Mass fluxes across standard pressure levels, averaged over the months July, August and September of years 1982, 1997 and 2015, and integrated over the standard zones of Fig. 4. Brackets indicate values when the northern boundary of the Cold Pool is set to 3°N. The mass flux units are $\mathrm{Tg\,s^{-1}}$

Pressure	200 hPa	500 hPa	800 hPa
Island Continent	−43.79	−56.92	−29.64
ITCZ (West)	−11.83	−27.64	−15.89
ITCZ	−25.43	−58.29	−55.73
	(−25.71)	(−60.71)	(−60.77)
EPWP	−13.64	−25.29	−22.16
	(−13.64)	(−26.54)	(−24.57)
SPCZ (West)	−5.41	−17.16	−12.08
SPCZ	1.18	−10.96	4.72
Equator	6.72	7.30	−1.52
	(7.00)	(11.02)	(5.92)
North Pacific	6.55	20.84	25.80
South Pacific	16.05	55.57	68.94
World	−0.02	−0.08	150.94

Changes at 500 and 300 hPa are broadly similar. In the Island Continent region, the area of sinking air associated with Australia expands at both levels. At the same time convection near the Equator moves eastwards, the region of maximum convection now lying between 150°E and 180°E.

Along the line of the ITCZ, convection is little changed at 500 hPa, but it is much stronger at 300 hPa. Thus, when strong El Niños are developing, convection in the ITCZ is no longer confined primarily to the lower atmosphere but instead has a much better probability of penetrating as far as the tropopause.

5.3 Quantitative Changes

The quantitative estimates of Tables 3 and 4, show that at 800 hPa, during the development of the strong El Niños, the largest change in convective flux occurs in the Island Continent region where it drops from 51 to 30 $\mathrm{Tg\,s^{-1}}$.

Elsewhere the relative changes are small. The ITCZ convective flux drops slightly, from 59 to 56 $\mathrm{Tg\,s^{-1}}$, and that of the East Pacific Warm Pool value, from 26 to 22 $\mathrm{Tg\,s^{-1}}$.

In the sinking regions, the largest change at 800 hPa is in the Equatorial zone, where a sinking rate of 29 $\mathrm{Tg\,s^{-1}}$ becomes a convective rate of 2 $\mathrm{Tg\,s^{-1}}$. Figure 12 shows there is still sinking air above the Equatorial Cold Pool, so the change probably reflects the changed positions of the ITCZ and the western Pacific convection region.

At 500 and 200 hPa the net convection over the Island Continent region is also reduced. However, relative to the value at 800 hPa there is little change at 500 hPa and a slight increase at 200 hPa. This indicates that although the total amount of convection in the region is reduced, the ability of the convective plumes to entrain air is not significantly affected.

The situation over the ITCZ is very different. Although at the surface the convective flux is little changed, at 500 hPa, instead of halving, the flux increases slightly to 58 $\mathrm{Tg\,s^{-1}}$. At 200 hPa, the flux is 25 Pg/s, twice the value in a normal year.

In the North and South Pacific sinking regions, the reduced fluxes at 500 and 200 hPa, reflect the changes at 800 hPa, the South Pacific being slightly anomalous in that it shows no change at 200 hPa. At the Equator there are significant drops in the rate of sinking, again probably a reflection in the movement of the surrounding convective regions.

In summary, main results from the quantitative estimates are, first, the significant reduction in the strength of convection over the Island Continent and, secondly, the penetration of convection in the ITCZ to high levels of the atmosphere.

5.4 Zonal Sections

Figure 13 shows that, between July and September during the development of the strong El Niños, the main convective region south of the Equator, which normally is close to New Guinea (Fig. 10) intensifies and moves eastwards. To the west the region of sinking air north-west of Australia expands in width, the eastern edge following the region of convection and the western edge passing 90°E at higher atmospheric levels. In the South Pacific, the zone of sinking air shows little change, and the same is true for the regions of rising and sinking air at other longitudes.

In the Equatorial band, between 5°S and 5°N, the changes are more substantial. In the Indonesian region, the low-level sinking regions near 110°E and 130°E, are more intensive during the developing El Niños, and result in a net sinking throughout the atmosphere.

The main convection region moves eastwards from the band between 130°E and 210°E, to 150°E and 220°E. Further east the sinking region over the Pacific Cold Pool is both

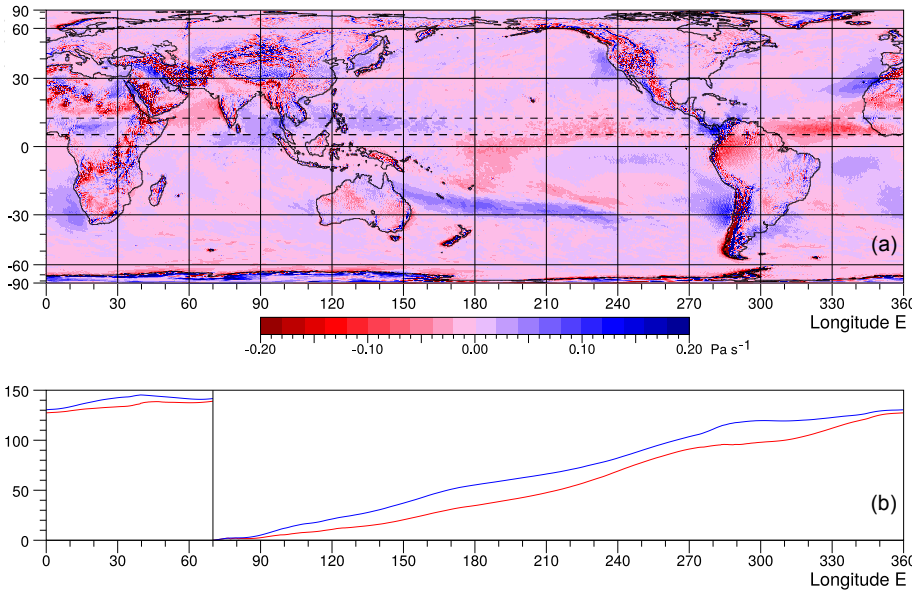

Figure 14. (a) The difference in the vertical flux between 300 hPa and 700 hPa averaged over months July, August and September of years 1982, 1997 and 2015. (b) Longitudinal integral of the vertical mass flux ($\mathrm{Tg\,s^{-1}}$) for the 700 hPa (red) and 300 hPa (blue) levels, calculated for the same time averaging period and integrated between 5°N and 12°N, and eastwards from 70°E to the longitude plotted.

reduced in size and shows a significant reduction in convection at all levels.

At other longitudes the changes are smaller, being limited to a slight increase in sinking rates over the South Atlantic at mid-levels and a slight increase in the entrained fluxes at mid-levels over the Indian Ocean.

In the band north of the Equator, the main change is an increase in convection at mid-levels at the longitudes of the ITCZ. There is a small change in the western boundary of the region, which moves from 190°E to 200°E, but the main region of convection, instead of decaying above 600 hPa, now continues up to the tropopause, with vertical velocities near 0.1 $\mathrm{Pa\,s^{-1}}$.

In the west Pacific, the centre of strong entrained convection between 125°and 145°E, intensifies and moves eastwards to lie between 140°E and 170°E. At other longitudes around the world in this band, changes are small.

Together the results from the zonal sections confirm the changed nature of convection above the ITCZ and changes to the convection in the bands along the Equator and south of the Equator. The main new point is the eastward movement of the region of enhanced convection in the west Pacific, which continues to entrain air high in the atmosphere. In addition, as the changes to the Hadley Cell stream function in all three bands are small, there might be a physical constraint that ensures that the zonal integrals remain roughly constant.

6 Conclusions

This preliminary analysis of the ERA5 data has shown that at low levels of the atmosphere, convection over the Island Continent is not as dominant as is sometimes implied. It has also shown that during the northern summer the greatest amount of low-level convection occurs along the line of the Inter-Tropical Convergence Zone and that six months later it is concentrated in the South Pacific Convergence Zone.

The study has shown that on average, most convection along the line of the ITCZ is limited to the lower half of the atmosphere. It has also shown that the convective flux over the Island Continent increases with height, as far as the tropopause, so that it becomes the dominant region of convection at 500 hPa and 300 hPa.

Although the SPCZ has the largest fluxes during the January to March period, the zonally integrated overturning stream function shows that the convective branch of the Hadley Cell starts at the surface north of the Equator. As the air rises, many of the stream function contours spread southwards across the Equator. This implies that although much of the ITCZ convection is only reaching mid-levels of the atmosphere, a large fraction of the detrained air is subsequently entrained by plumes south of the Equator.

The study investigated the changes, that occur in the Pacific, during the development of the strong El Niños of 1982-83, 1997-98 and 2015-16. Previous studies (Webb, 2018, 2021; Webb et al., 2020) concluded that, while the El Niños are developing, the North Equatorial Counter Current carries water warm enough to trigger deep atmospheric convection into the central and eastern Pacific.

The present results show that, during this period, the convective flux near the surface falls slightly, from 59 to 55 $\mathrm{Tg\,s^{-1}}$. As the convection is hardly changed, the increased SST can have little effect on near surface winds and so is unlikely to have a direct impact on other aspects of the ocean's El Niño response.

Instead, the increased SST values result in the ITCZ extending much higher in the atmosphere. At 500 hPa con-

vection increases from 35 to 58 $\mathrm{Tg\,s^{-1}}$ and at 200 hPa it increases from 12 to 25 $\mathrm{Tg\,s^{-1}}$. The results imply that if increased SST values are having a wider impact on El Niños, it is through the large-scale overturning of the atmosphere.

In this respect, it is noticeable that, during the development of strong El Niños, convection over the Island Continent is severely reduced, from 51 to 30 $\mathrm{Tg\,s^{-1}}$ at 800 hPa and from 104 to 57 $\mathrm{Tg\,s^{-1}}$ at 500 hPa. The reduced convection at low levels will affect near-surface winds and could result in reduced easterlies over the western equatorial Pacific.

6.1 Physics and Causality

Although the results show several apparent correlations between different components of the system, care needs to be taken when discussing causality.

In the case of the correlation between a warmer NECC and strong El Niños, both are rare events, so the probability of the three strong El Niño events occurring when the NECC just happens to be warmer than normal is small. The warming of the NECC occurs before the strong El Niño develops, implying a possible causal relation.

Warmer sea surface temperatures along the line of the NECC would, on physical grounds, be expected to affect convection in the adjacent ITCZ. This might increase the rate of convection or it's vertical penetration. The present results indicate that the rate of convection decreases slightly, so any changes in the surface wind field is unlikely to significantly change the winds along the Equator and so trigger an El Niño.

Instead, the results show that ITCZ convection does penetrate more, so it is probable that this is a result of the increased sea surface temperatures. The change in penetration will affect the balance of fluxes at mid-levels of the atmosphere but it is not obvious how this may relate to the generation or development of El Niños.

During the development of the strong El Niños convection is reduced in the Island Continent region, and although this might affect surface winds and the position of strong convection in the nearby western Pacific, it is again not obvious how it may be the result of the changes in the NECC and ITCZ.

Overall, the results have shown that the NECC could influence the large-scale circulation of the atmosphere, and thus the El Niño, via its effect on the ITCZ. At the same time none of the other changes observed during the development of the strong El Niños, appear insufficient to explain the increased temperatures of the NECC.

The results of the study have also highlighted the important roles of detrainment and entrainment in the large-scale circulation of the equatorial atmosphere. This processes are not normally included in discussions of the Hadley Cells, the Walker cells or El Niños. However, the balance between the two processes appears to be important and, without entrainment, divergence above the Island Continent would be severely reduced.

As a final point, the results of this study depend heavily on the accuracy of the ERA5 reanalysis data. This in turn depends on the accuracy of the raw data, the quality of the model and the quality of the assimilation scheme. The model and assimilation scheme are tested by every forecast provided by the ECMWF and are unquestionably very good.

The data for the Pacific has improved significantly during the period studied, due to the extra range and quality of satellite observations. It would be good to have some independent confirmation of the present results, but for the moment there appears to be no reason to doubt the main results and conclusions.

Acknowledgements. The present study was carried out at the National Oceanography Center, UK, and funded by NERC, the Natural Environment Research Council. The atmospheric data was generated by the European Centre for Medium-Range Weather Forecasts and provided for analysis by the Copernicus Climate Change and Atmosphere Monitoring Services (Hersbach et al., 2022).

References

Blunden, J. and Arndt, D. S., eds.: State of the Climate, vol. 97, https://doi.org/10.1175/2016BAMSStateoftheClimate.1, 2016.

Clarke, A. J.: El Niño Physics and El Niño Predictibility, in: Annual review of Marine Science, vol. 6, pp. 79–99, Annual Reviews, 2014.

Cubukcu, N. and Krishnamurti, T. N.: Low-Frequency Controls on the Thresholds of Sea Surface Temperature over the Western Tropical Pacific, Journal of Climate, 15, 1626–1642, 2002.

Dima, I. M. and Wallace, J. M.: On the Seasonality of the Hadley Cell, Journal of Atmosheric Sciences, 60, 1522–1527, 2003.

ECMWF: IFS Documentation CY41R2 - Part III: Dynamics and Numerical Procedures, Tech. rep., European Centre for Medium-Range Weather Forecasts, Shinfield Park, Reading, RG2 9AX, England, https://doi.org/10.21957/83wouv80, 2016a.

ECMWF: IFS Documentation CY41R2 - Part IV: Physical Processes, Tech. rep., European Centre for Medium-Range Weather Forecasts, Shinfield Park, Reading, RG2 9AX, England, https://doi.org/10.21957/tr5rv27xu, 2016b.

Evans, J. L. and Webster, C. C.: A variable sea surface temperature threshold for tropical convection, Australian Meteorological and Oceanographic Journal, 64, S1–S8, https://doi.org/10.22499/2.6401.007, 2014.

Feng, J., Li, J., Jin, F.-F., Liu, Z., and Zhao, S.: Effect of El Niño on the reponse ratio of Hadley circulation to different SST meridional structures, Climate Dynamics, 53, 3877–3891, https://doi.org/10.1007/s00382-019-04756-7, 2019.

Gadgil, S., Joseph, P. V., and Joshi, N. V.: Ocean-atmosphere coupling over monsoon regions, Nature, 312, 141–143, 1984.

Guo, Y.-P. and Tan, Z.-M.: Relationahip between El Niño- Southern Oscillation and the Symmetry of the Hadley Circulation Role in the Sea Surface Temperatue Annual Cycle, Journal of Climate, 31, 5319–5332, https://doi.org/10.1175/JCLI-D-17-0788, 2018.

Hastenrath, S.: Meteorology and Atmospheric Physics, 71, 243–254, 1999.

Held, I. and Hou, A.: Nonlinear axially symmetric circulations in a nearly inviscid atmosphere, Journal of the Atmospheric Sciences, 37, 515–533, https://doi.org/10.1175/1520-0469(1980)037<0515:NASCIA>2.0.CO;2, 1980.

Hersbach, H., Bell, B., Berrisford, P., Biavati, G., Horányi, A., Muñoz Sabater, J., Nicolas, J., Peubey, C., Radu, R., Rozum, I., Schepers, D., Simmons, A., Soci, C., Dee, D., and Thépaut, J.-N.: ERA5 monthly averaged data on pressure levels from 1940 to present., https://doi.org/10.24381/cds.6860a573, 2022.

Hoskins, B. and Yang, G.-Y.: The Detailed Dynamics of the Hadley Cell. Part II: December–February, Journal of Climate, 34, 805–823, https://doi.org/10.1175/JCLI-D-20-0504.1, 2021.

Hoskins, B., Yang, G.-Y., and Fonseca, R.: The detailed dynamics of the June–August Hadley Cell, Quarterly Journal of the Royal Meteorological Society, 146, 557–575, https://doi.org/10.1002/qj.3702, 2020.

Ji, X., Feng, J., Li, J., and Chen, X.: Relationship between the hadley circulation and the SST meridional structures under differetn thermal conditions in the indo-pacific warm pool, Frontiers in Marine Science, p. 1088276, https://doi.org/10.3389/fmars.2022.1088276, 2023.

Kubar, T. L. and Jiang, J. H.: Net Cloud Thinning, Low-Level Cloud Diminishment, and Hadley Cell Weakening of Precipitation Clounds with Tropical West Pacific SST Using MISR and Other Satellite and Reanalysis Data., Remote Sensing, 1250, 33, https://doi.org/10.3390/rs11101250, 2019.

Li, Y., Xie, S.-P., Lian, T., Zhang, G., Feng, J., Ma, J., Peng, Q., and Wang, W.: Interannual Variability of Regional Hadley Circulation and El Niño Interaction, Geophysical Research lettrs, 50, e2022GL102 016, https://doi.org/10.1029/2022GL102016, 2023.

Li, Z. and Fedorov, A. V.: Coupled dynamics of the North Equatorial Countercurrent and Intertropical Convergence Zone with relevance to the double-ITCZ problem, PNAS, 119, 9, https://doi.org/10.1073/pnas.212039119, 2022.

Lindzen, R. S. and Hou, A. Y.: Hadley Circulations for Zonally Averaged Heating Centered off the Equator, Journal of the Atmospheric Sciences, 45, 2416–2427, 1988.

McPhaden, M.: Genesis and Evolution of the 1997-98 El Niño, Science, 283, 950–954, https://doi.org/10.1126/science.283.5404.950, 1999.

McPhaden, M. J., Santoso, A., and Cai, W., eds.: El Niño Southern Oscillation in a Changing Climate, American Geophysical Union, ISBN ISBN 9781119548126, 2020.

Oort, A. H. and Rasmusson, E. M.: On the Annual Variation of the Monthl Mean Meridional Circulation, Monthly Weather Trview, 98, 423–442, 1970.

Oort, A. H. and Yienger, J. J.: Observed Interannual Variability of the Hadley Circulation and its Connection to ENSO, Journal of Climate, 9, 2751–2767, 1996.

Philander, S.: El Niño and La Niña, Journal of Atmospheric Sciences, 42, 2652–2662, 1985.

Philander, S. G. H.: El Niño Southern Oscillation phenomena, Nature, 302, 295–301, https://doi.org/10.1038/302295a0, 1983.

Picaut, J., Ioualalen, M., Menkes, C., Delcroix, T., and McPhaden, M. J.: Mechanism of the Zonal Displacements of the Pacific Warm Pool: Implications for ENSO, Science, 274, 1486–1489, https://doi.org/10.1126/science.274.5292.1486, 1996.

Qian, J.-H.: Why Precipitation is Mostly Concentrated over Islands of the Maritime Continent, Journal of the Atmospheric Sciences, 65, 1428–1441, 2008.

Santoso, A., McPhaden, M., and Cai, W.: The Defining Characteristics of ENSO Extremes and the Strong 2015/2016 El Niño, Reviews of Geophysics, 55, 1079–1129, https://doi.org/10.1002/2017RG000560, 2017.

Sun, Y., Li, L. Z. X., Ramstein, G., Zhou, T., Tan, N., Kageyama, M., and Wang, S.: Regional meridional cells governing the interannual variability of the Hadley circulation in boreal winter, Climate Dynamics, 52, 831–853, https://doi.org/10.1007/s00382-018-4263-7, 2019.

Takahashi, K. and Battisti, D. S.: Processes Controlling the Mean Tropical Pacific Precipitation Pattern. Part I: The Andes and the Eastern Pacific ITCZ, Journal of Climate, 20, 3434–3451, 2007.

Tiedtke, M.: A comprehensive mass flux scheme for cumulus parameterization in large-scale models, Monthly Weather Review, 117, 1779–1800, 1989.

Tiedtke, M.: Representation of clouds in large-scale models, Monthly Weather Review, 121, 3040–3061, 1993.

Webb, D. J.: On the role of the North Equatorial Current during a strong El Niño, Ocean Science, 14, 633–660, https://doi.org/10.5195/os-14-633-2018, 2018.

Webb, D. J.: On the low western Pacific sea levels observed prior to strong East Pacific El Niños, Ocean Science, 17, 1585–1604, https://doi.org/10.5194/os-17-1585-2021, 2021.

Webb, D. J., Coward, A. C., and Snaith, H. M.: A comparison of ocean model data and satellite observations of features affecting the growth of the North Equatorial Counter Current during the strong 1997–1998 El Niño, Ocean Science, 16, 565–574, https://doi.org/10.5195/os-16-565-2020, 2020.

Zhou, C., Lu, J., Hu, Y., and Zelinka, M. D.: Respone of the Hadley Circulation to Regional Sea Surface Temperature Changes, Journal of Climate, 33, 429–441, https://doi.org/10.1175/JCL-D-19-0315.s1, 2020.

National Oceanography Centre, European Way, Southampton, SO14 3ZH
United Kingdom +44 (0)300 131 2321

Joseph Proudman Building 6 Brownlow Street, Liverpool, L3 5DA
United Kingdom +44 (0)151 795 4800

National Oceanography Centre is a company limited by guarantee, set up under the law of England and Wales, company number 11444362.

National Oceanography Centre is registered as a charity in England and Wales, charity number 1185265, and in Scotland, charity number SC049896.

NOC.AC.UK